Thermochimica Acta 690 (2020) 178662

Contents lists available at ScienceDirect

Thermochimica Acta

journal homepage: www.elsevier.com/locate/tca

Thermal analysis combined with X-ray diffraction/Rietveld method, FT-IR and UV-vis spectroscopy: Structural characterization of the lanthanum and cerium (III) polycrystalline complexes

K.V. Tenorio[a], A.B. Fortunato[a], J.M. Moreira[a], D. Roman[a], K.A. D'Oliveira[b], A. Cuin[b], D.M. Brasil[c], L.M.C. Pinto[c], T.A.D. Colman[a], C.T. Carvalho[a,*]

[a] Federal University of Grande Dourados, UFGD, CP 364, 79.804-970, Dourados, MS, Brazil
[b] Federal University of Juiz de Fora, UFJF, 36036–330, Juiz de Fora, MG, Brazil
[c] Federal University of Mato Grosso do Sul, 79074-460, Campo Grande, MS, Brazil

ARTICLE INFO

Keywords:
Synthesis
Thermal analysis
X-ray diffraction
Polymeric structure
Theoretical calculation

ABSTRACT

In this work, structural, spectroscopical and thermal studies of lanthanum(III) and cerium(III) complexes with the 3,5-dimethoxybenzoate (DMBz) monocarboxylate ligand were performed. The metal-ligand minimum stoichiometry and polymeric arrangement of the complexes were respectively defined by TGA-DSC and X-ray powder diffraction as $[M(DMBz)_3.n]x$, wherein "M" represents the lanthanides, "n" the water molecules in the lanthanum compound and "x" the basic unit of repetition in monoclinic polycrystalline system with space group $P2_1/c$. The products of the thermal decomposition of the material were also monitored by TGA-DSC/FT-IR both in air and N_2 atmospheres in order to suggest the thermal decomposition mechanism. Theoretical calculations based in experimental results were performed to assess the coordination mode and spectroscopic properties of lanthanide complexes involving a monocarboxylate ligand. From theoretical calculations it was possible to generate FT-IR theoretical vibrational spectra and relate the level of correspondence to the experimental data inherent to the metal-ligand coordination mode. From the HOMO/LUMO orbitals obtained by TD-DFT calculations, the main electronic transitions responsible for the absorption and emission bands of the complexes were determined.

- TGA/DSC/FT–IR analysis and refinement by Rietveld method
- Polymeric structure of monoclinic system with space group P21/c
- Elucidation of the type of carboxylate-metal coordination in the complexes
- Computational calculations
- HOMO – LUMO molecular orbital contributions

1. Introduction

Lanthanides complexes obtained with carboxylate ligands in their structure have been extensively studied in the solid state. Characterization of most of these compounds has been done using thermal analysis techniques, mainly thermogravimetric, to establish the dehydration grade, thermal stability, thermal behavior, stoichiometric and purity, as well as infrared spectroscopy (FT-IR) technique to provide information concerning the coordination mode of mono or dicarboxylate ligands to the lanthanides. Among the research groups with an expressive number of scientific papers published on lanthanide carboxylates, it is worth mentioning those of the researchers Ionashiro and Ferenc and their collaborators, represented here by the references [1–3], which can support some of the characterizations used in this study.

In recent years, metal carboxylates, often referred to as coordinating polymers [3], have attracted interest from the scientific community around the world since they can be used to produce a fascinating class of materials, the MOFs (Metal-Organic Frameworks), promising structures for application in catalysis, gas separation, gas storage, ion exchange, luminescence, among others [4,5]. For application of these materials, it is equally interesting to know their structural arrangement, however, in most cases they are difficult to be obtained due to the absence of single crystals [1–4]. One way researchers have found to overcome this is by adding a nitrogenous co-ligand in the synthesis

---

[*] Corresponding author.
E-mail address: claudiocarvalho@ufgd.edu.br (C.T. Carvalho).

https://doi.org/10.1016/j.tca.2020.178662
Received 9 March 2020; Received in revised form 12 May 2020; Accepted 23 May 2020

process [6,7]. In such syntheses, the researchers Zheng and collaborators and Ling-Yan and collaborators added the 2,2′-bipyridine and 1,10-phenanthroline co-ligands respectively, so that through this methodology they were able to obtain crystalline complexes. These materials were then characterized using x-ray diffraction for single crystal, thermal and spectroscopic techniques, as well as kinetic and luminescence studies.

On the other hand, the synthesis of complexes using only carboxylate ligands to obtain single crystals can also be found in the literature. Those syntheses carried out under hydrothermal conditions are made under high temperature and pressure, however it is not always easy to obtain crystals through this method [8,9].

Finally, an elegant way of elucidating the structure of metallic complexes obtained in powder form is using the Rietveld method for analysis of crystalline parameters.To take full advantage of this method in providing reliable information, though, it is important to make previous use of an appropriate thermogravimetric characterization to determine the stoichiometry of the material, especially carried out under air atmosphere, so that the XRD theoretical and experimental data obtained are convergent. In this sense, Katia and collaborators [10] using the 3,5-dimethoxybenzoate ligand as complexing agent for the praseodymium metal obtained this compound in the form of crystalline powder and resolved its structure combining theoretical calculations, TGA-DSC characterization techniques and powder X-ray diffraction (XRD) analysis and refinement by the Rietveld method.

Another study can be cited to exemplify this application, which is that of Roel and collaborators [5]. They synthesized lanthanide complexes using two different types of dicarboxylate ligand so that one compound was obtained in the form of monocrystal using hydrothermal synthesis, while another four compounds were obtained in the form of crystalline powder. The elucidation of the structures of the compounds, obtained in powder form, was solved using the Rietveld method accompanied by thermal and spectroscopic characterizations, as well as porosity analysis.

Based on the results presented in the literature and given the absence of studies on the elucidation of the crystalline structure of the 3,5 lanthanum(III) and cerium(III) dimethoxybenzoates in the literature, we were motivated to synthesize and characterize them using thermal and spectroscopic techniques as a basis for elucidation of the structure of these materials using X-ray powder diffraction and refinement by the Rietveld method. From the result obtained, other important theoretical-experimental correlations were evaluated using experimental and theoretical FT-IR data and Time-Dependent Density Functional Theory (TD-DFT) calculations in order to obtain insights related to the optical properties of the materials, not found in the literature, for future applications.

2. Experimental

2.1. Synthesis of the complexes

The DMBz, 3,5-dimethoxybenzoic acid $(CH_3O)_2C_6H_3CO_2H$ 97 % purity, was purchased from Sigma-Aldrich Brazil. For the synthesis, a solution of 0.100 mol L^{-1} of sodium salt [NaDMBz] was prepared at the pH of 8.0 from the DMBz acid using a 0.100 mol L^{-1}NaOH solution, whereas the metal salts (chloride or nitrate) solutions were prepared from lanthanum oxide with concentrated hydrochloric acid and from cerium nitrate by direct dissolution, both at the pH adjusted between 5 and 6. The pH measurements were assisted by a pH-meter with glass electrode [10]. Approximately 500 milligrams of each complex [M $(DMBz)_3$] in solid state, wherein M = lanthanum or cerium, were obtained by mixing both solutions at 27 °C so that the slight excess of the ligand aqueous solution was used until complete precipitation of the rare earth ion. The precipitate obtained was washed with distilled water for elimination of chloride or nitrate and sodium ions and filtered through Whatman® quantitative filter paper (Grade 42). After washing, the precipitate was dried in an oven at 60 °C for 10 h and then kept stored in a desiccator until the moment of the analyses.

2.2. Instrumental analysis

FT-IR/ATR spectra of the [NaDMBz] salt and complexes were performed using a Nicolet iS10 FT-IR spectrophotometer using ATR accessory with Ge window.

The TGA-DSC curves were obtained using a thermal analytical system, model STA 449 F3 Jupiter® and the experimental data were obtained by Proteus® Software. For the analysis of the samples, masses near to 10 mg and alumina crucibles under purge gas flow (air or N_2) of 50 ml min^{-1} with heating rate optimized to 10 °C min^{-1} were used.

The percentages of carbon, hydrogen, oxygen and metal were determined by the mass losses data in TGA curves, since the decomposition of the complexes occurs with total thermal decomposition of the organic content and further production of the respective metal oxides of known stoichiometry, La_2O_3 and CeO_2.

The gaseous fragments of the thermal decomposition of the complexes were monitored using a Mettler® TGA-DSC system coupled to a Nicolet® FT-IR spectrophotometer equipped with gas cell and DTGS KBr detector. The gas cell was kept at 250 °C and the 120 cm transfer line at 225 °C. The mass of the samples for the TGA-DSC curves recording were about 10 mg with heating rate of 10 °C min^{-1} in alumina crucibles. The online FT-IR spectra were recorded at 4 cm^{-1}resolution.

The sample image (DSC video) was obtained by the Mettler-Toledo DSC 1 Stare System equipment with a SC30 digital camera which incorporates a 3.3 Megapixel CMOS sensor, Navitar 1-6232D mechanical optical subassembly with 6.5X zoom. The sample mass used was approximately 2 mg heated at the ratio of 10 °C min^{-1}.

2.3. Crystal structure

The $[La(DMBz)_3{\cdot}2H_2O]$ complex, before being analyzed by powder X-ray diffraction, was dehydrated at 200 °C in a muffle furnace, temperature selected according to TGA-DSC previous data. Then, the $[La(DMBz)_3]$ and $[Ce(DMBz)_3]$ samples were carefully grounded in an agate mortar and measured by powder diffraction methods, depositing them on a glass sample-holder plate. The diffraction data were collected by overnight scans in the 2θ range of 5 − 105° with step of 0.02°, using a Bruker AXS D8 Da Vinci Advanced diffraction equipped with Ni-filtered CuK_α radiation (λ = 1.5418 Å) and Lynxeye linear position-sensitive detector (2.94°).The optical parameters were primary-beam Soller slits (2.94°), fixed divergence slit (0.3°) and receiving slit 8.0 mm. The unit cell parameters were checked using about 20 low-angle peaks, followed by indexing through the single-value decomposition approach by Coelho [11,12]. The space group $P2_{1/c}$ was chosen for both complexes and after checking the systematic absences and the cell parameters, they were then refined using diffraction data up to the range of 55° (2θ) using Pawley method [13]. In both cases, no higher symmetry transformations were suggested by Spek [14]. The structure solution process of each complex was performed by the simulated annealing technique [15], also implemented in TOPAS. The 3,5-dimethoxybenzate ion rigid body model based on single-crystal data [16] was defined by the Z-matrix formalism, Fig. 1, as well as in previous works [17,18].

The optical and specimen parameters and angles of torsion, translation and rotation of the lanthanide ions and ligands were adjusted by the Chebyshev polynomial function and refined by the Rietveld method [19]. The crystal structure models found were treated by SA routine in conjunction with new assays. The final Rietveld refinement plots of both complexes are described as supplementary material, Fig. S1a and S1b.

Absorption spectra in the ultraviolet/visible region were recorded using a Digital UV/Visible scanning spectrophotometer, Model IL-592S-BI – KASUAKI, in wavenumber range of 190–1000 nm and spectral band width of 2 nm.

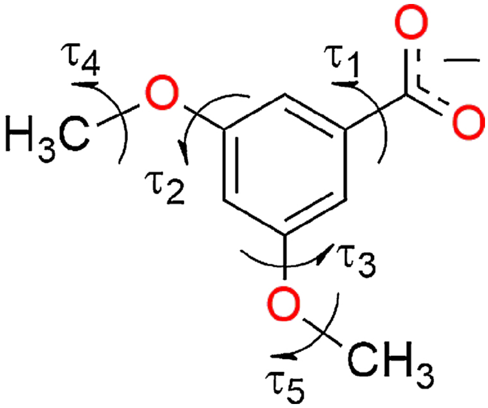

Fig. 1. Sketch of the 3,5-dimethoxybenzate ion. The 5 torsion angles required in the simulated annealing and refinement routines were defined as τ_1 to τ_5.

For the fluorescence studies, a Varian Cary Eclipse spectrofluorimeter was used applying an excitation scan in the range of 210 nm–600 nm at intervals of 10 nm. A xenon lamp with two monochromators was used as excitation source, one of which was intended to select the excitation wavelength and the other to select the wavelength emitted by the sample, with fluorescence detection by a photomultiplier tube. Solutions containing 5 mg of each compound in *N,N*-dimethylformamide (DMF) 99 % purity (J.T. Baker) were analyzed at the temperature of 25 °C.

For the FT-IR theoretical calculation, the quantum chemical approach employed to determine the molecular structure was Becke's three parameter hybrid exchange functional combined with Lee-Yang-Par correlation functional (B3LYP) [20,21]. The molecular calculations in this study were made using the Gaussian 09 routine [22] and the theoretical infrared spectrum was calculated using a harmonic field [23,24] based on C1 symmetry (electronic state 1A). The geometry optimization was computed using the Berny's optimization algorithm and the calculations of vibrational frequencies were also implemented to determine whether the optimized geometry constitutes minimum or saddle points. The principal assignments and descriptions of the infrared active fundamental mode were provided by Gauss View 5.0.2 W graphic routines [25].

Absorption theoretical calculations were performed within TD-DFT using the def2-SVP [26] basis set for the light atoms (C, O, and H), and the def2-TZVP [26] for the lanthanides with the Stutttgart-Dresden ECP (MBW28) for lanthanum [27] and (MBW47) for cerium [27,28] implemented in the ORCA 4.0.1 package (Neese F 2012). Molecular orbital diagrams were reproduced using Avogadro (version 1.2.0) [29,30].

3. Results and discussion

3.1. Thermal study

The TGA-DSC/DTG thermal analyses data, Fig. 2, under air and inert (N_2) atmospheres are shown in the summary form in Table 1 and Table S1 in supplementary material, so that it is possible to make a more accurate analysis of the material studied as follows. For the lanthanum complex under air atmosphere, a mass loss starting at 64 °C (TGA/DTG) is observed, which is associated with a small endothermic peak in the DSC at 91 °C. This event can be attributed to dehydration that occurs in a single step and through a slow process. After this mass loss step, the complex in the anhydrous form is thermally stable over a wide temperature range.

Therefore, from this point onwards the description of the thermal events for both complexes can be summarized in anhydrous form. Thus, by examining the TGA-DSC/DTG curves in the air atmosphere it can be stated that the complexes in their anhydrous form are thermally stable up to around 326 °C (La) and 315 °C (Ce). Above those temperatures, the thermal decomposition of the ligand occurs basically in two stages of mass loss. In these processes, a fact to be highlighted is that the thermal decomposition of the cerium complex occurs in a temperature range lower (315–381 °C) than that for the lanthanum complex (326–401 °C). Based on these experimental data, it can be suggested that the result shown is intrinsically linked to the change of the oxidation state of cerium metal from 3+ to 4+ during the thermal decomposition. This exothermic process probably occurs simultaneously with the decomposition of the organic matter (intense peak at 371 °C), so that it helps raising the temperature inside the sample and concomitantly contributes to the thermal decomposition of the organic matter occurring at a lower temperature and through a fast process when compared to other lanthanide ions complexed with the same ligand. These data can be observed in other studies [2,31,32].

The last two steps of mass loss (TGA/DTG) for lanthanum complex, which comprise a slow mass loss between 401 and 639 °C, is related to thermal decomposition of the carbonized material without peak associated with the DSC and DTG curves, while the mass loss between 639 and 700 °C, associated with an endothermic peak at 673 °C, is related to carbonate decomposition from the dioxycarbonates ($La_2O_2CO_3 \rightarrow La_2O_3 + CO_2$) mixture. In this reaction, as CO_2 is stable under oxidizing atmosphere, it is concluded, based on thermodynamic laws, that the absorbed energy (bond breaks) is greater than the energy released (product formation), that is, with delta H > 0 for this system. This thermal event at 673 °C can be better observed by the 5x magnified image on the y-axis for the DSC curve inserted in Fig. 2. In addition, dioxycarbonates formation, especially for the lanthanum metal coordinated to carboxylate ligands, is common to occur, so that a qualitative test of the residue, obtained at this temperature with diluted HCl solution was used to indicate the presence of carbonate [2,31]. For cerium complex, the last step between 381 and 560 °C (TGA) occurs associated with an exotherm (similar to an extended exothermic peak) in DSC curve between 465 and 550 °C. Furthermore, similarly to the slow stage of mass loss for lanthanum compound, the DTG curve also does not peak in this region, because gradual changes are produced without an inflection point. Lastly, considering the end of the steps for each of the complexes, the residues formed were the La_2O_3 and CeO_2 oxides, which at high temperatures and in an oxidizing atmosphere (air) are obtained free of carbonaceous material. Therefore, from the experimental results obtained using an oxidizing atmosphere in relation to the percentages of water loss, ligand and oxide formation per step (Table 1), when compared to the theoretical results (Table S1), it was possible to establish the empirical formula of these compounds as follows: $[La(DMBz)_3 \cdot 2H_2O]$ and $[Ce(DMBz)_3]$.

TGA-DSC/DTG analysis (Fig. 2) in N_2 inert atmosphere for the complexes shows a different profile of the curves when compared to that presented in air atmosphere. This difference is due to the interaction of oxygen with the released volatiles, resulting in degradation and/or combustion of the organic matter, while in nitrogen atmosphere there is only energy transference (heat) to the substance with higher production of volatile compounds at high temperatures. On the other hand, the thermal events related to the hydration water will always have similar profiles under both atmospheres. This observation ratifies the explanation of the interaction between the atmosphere and the volatile products, since the loss of hydration water only requires energy absorption. In relation to the thermal events of the second step, the differences in the decomposition profile of the organic matter (ligand) are significant under air and N_2. Under air atmosphere, it is possible to observe intense exothermic peaks, while in N_2 atmosphere; endothermic peaks of low intensity are noticed.

Another interesting result observed only in N_2 inert atmosphere is the sharp endothermic peak at 356 °C (La) in the DSC curve, Fig. 2, with no corresponding mass losses in the TGA/DTG curves. This type of event, identified as a physical one, is due to the phase transition of the

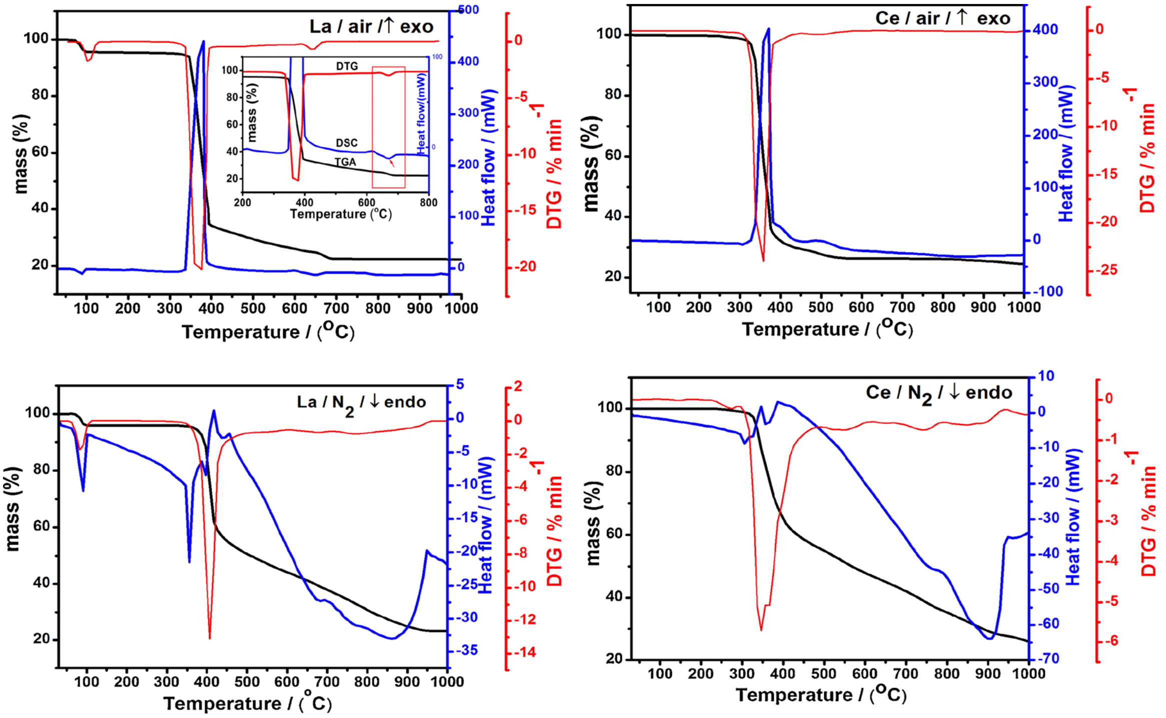

Fig. 2. TGA-DSC/DTG curves in air (for stoichiometry) and N_2 (pyrolysis) atmospheres using a heating ratio of 10 °C min^{-1} and initial mass near 10.0 mg for lanthanum and cerium complexes study. Peaks up (exo) and peaks down (endo).

lanthanum complex in its anhydrous form, as elucidated by DSC analysis coupled to a microscope shown in the video (supplementary material). In addition, the endothermic peaks at 396 and 436 °C (DSC) are probably related to the thermal decomposition/pyrolysis of the organic matter, which occurs within a single rapid step according to DTG peak, between 350 and 439 °C. Thus, examining the relationship between the thermal events observed in the DTG and DSC curves, it can be suggested that the rapid decomposition in this region seems to be favored by the physical event. The last mass loss step, above 439 °C without DTG peak, is related to the thermal decomposition of the pyrolyzed material (carbonaceous material), which is signaled by simultaneous endothermic events in the DSC curve between 670 and 943 °C.

Considering the first thermal decomposition step of the cerium complex, between 262–416 °C (TGA), unlike lanthanum complex, it is possible to observe three endothermic peaks in this region (DSC), being the first two at 306 and 326 °C overlapped, which coincide with a small mass loss in the TGA curve, as well as with the beginning of the opening of two large overlapping DTG peaks, Fig. 2. Thus, it is possible that the beginning of the thermal decomposition is associated with decarboxylation in parallel to the mass losses of the methoxy groups of the ligand, while the adjacent step with DSC peak at 356 °C and overlapping DTG peak (364 °C) can be possibly attributed to the thermal decomposition/pyrolysis of the organic matter, remaining aromatic residue. The last step, between 416 and 1000 °C (TGA) and without a defined

Table 1
TGA-DSC/DTG thermoanalytical data of the lanthanum and cerium complexes performed in air and N_2 atmospheres, where the mass losses and metal oxides formed in air were used for stoichiometric calculus.

Steps of mass loss	Events	$[La(DMBz)_3{\cdot}2H_2O]$ air	$[La(DMBz)_3{\cdot}2H_2O]$ N_2	$[Ce(DMBz)_3]$ air	$[Ce(DMBz)_3]$ N_2
1st	**θ ºC**	64 – 100	72 – 102	299 – 381	262 – 416
	***mg (%)**	0.45 mg (4.50 %)	0.41 mg (4.10 %)	6.61 mg (66.10 %)	3.8 mg (38.00 %)
	Tp (ºC)	91↓	91↓	371↑	306↓, 326↓,356↓
2nd	**θ ºC**	326 – 401	350 – 439	381 – 560	416 – 1000
	***mg (%)**	6.12 mg (61.30 %)	4.159 mg (41.59 %)	0.82 mg (8.20 %)	3.61 mg (36.10 %)
	Tp (ºC)	392↑	356↓↓, 396↓, 436↓	465 – 550 exotherm	909↓
3rd	**θ ºC**	401 – 639	439 – 943	–	–
	***mg (%)**	0.855 mg (8.55 %)	3.101 mg (31.01 %)	–	–
	Tp (ºC)	–	–	–	–
4th	**θ ºC**	639 – 700	–	–	–
	***mg (%)**	0.315 mg (3.15 %)	–	–	–
	Tp (ºC)	673↓	–	–	–
Residue	***mg (%)**	La_2O_3 2.25 mg (22.50 %)	La_2O_3 2.33 mg (23.30 %)	CeO_2 2.57 mg (25.70 %)	$CeO_2 + R$ 2.59 mg (25.90 %)

Temperature range (θ), *mass loss observed in TGA curves in milligrams (mg) and percentage (%), peak temperature (Tp) observed in DSC curves, exothermic event↑, endothermic event↓, phase transition↓↓. DMBz = 3,5-dimethoxybenzoate and R = carbonaceous residue.

peak in the DTG, but with a wide and intense peak at 909 °C is due to partial decomposition of the pyrolyzed material.

In summary, from the TGA-DSC/DTG data in both atmospheres it was possible to observe physical and chemical events such as: thermal behavior, stoichiometric ratio of the complexes, phase transition, thermal stability, decomposition steps and stable residue formation temperature. For the identification of the decomposition products released in each step, a TGA-DSC/FT-IR system was used. Specifically for this analysis type, the nitrogen atmosphere is more efficient than the air atmosphere, since in air the fragmentation of the organic matter leads to an excessive production of carbon monoxide (CO) and carbon dioxide (CO_2), so that these excess can overlap the bands of organic fragments.

3.1.1. EGA - evolved gas analysis

In parallel with the thermal behavior study and stoichiometry determination by TGA-DSC, we also monitored the gaseous products from thermal decomposition in air and nitrogen atmospheres through a TGA-DSC/FT-IR system, so that in both atmospheres the same products were detected. However, as previously mentioned, the monitoring of gaseous products is more advantageous in an inert atmosphere because the amount of CO and CO_2 produced from the organic matter decomposition is lower, i.e., inherent only to the ligand decarboxylation. The combination of these results now offers us the possibility of obtaining a set of complementary information about the complexes that can be used to evaluate the likely thermal decomposition mechanism those complexes follow.

The gaseous products of the thermal decomposition of the complexes [La$(DMBz)_3$] and [Ce$(DMBz)_3$] in anhydrous form, Fig. 3 (a–d), were continuously monitored between 30 and 1000 °C (TGA). The experimental FT-IR spectra obtained were compared with literature data [33,34] as well as evaluated and compared through OMNIC® software with a broad spectral library of gaseous products. The bands identified in FT-IR spectra (numbered 1–6), Fig. 3(a–d), are also associated with illustrations of the possible position of fragmentation in the molecule of the ligand (1*, 2*, 3* and 4*). Among the products monitored under air atmosphere, observed in a relatively larger quantity, the fragments of two groups released simultaneously in the first mass loss steps (TGA) up to 360 °C stand out, which are methanol (CH_3OH), with peaks at 1008, 1033 e 1062 cm^{-1} originating from methoxy groups, and carbon dioxide (CO_2), Fig. 3(a), with characteristic peaks in doublet form at 2360, 2400 cm^{-1} and 666 cm^{-1}, assigned to the decarboxylation of the carboxylate group. In addition to these two main fragments, there is also the presence of peaks of very small intensity, inherent to fragments of dimethoxybenzene ($C_8H_{10}O_2$) with bands at 1046, 1150, 1202, 1286, 1486 and 1594 cm^{-1}, and methoxybenzene (C_7H_8O) with bands at 1054, 1254, 1498, 1602 cm^{-1} and 1062 cm^{-1}, as shown in Fig. 3 (b, c). From 360 °C, an increase in the proportion of CO_2 in relation to the other products is observed, so that from the slow mass losses steps at 401 °C (La) and 381 °C (Ce), Fig. 3(d), only methane (peaks at 2995 and 3018 cm^{-1}) and carbon dioxide (CO_2) are observed in the FT-IR spectra. Possibly, most of the gaseous products CH_4 and CO_2 originate from the fragmentation of the carbon skeleton.

The monitoring in nitrogen atmosphere, slightly different from that observed in air atmosphere, initially shows methanol as the only product released and, as mentioned earlier, it comes from the methoxy group of the ligand. This process occurs almost simultaneously with decarboxylation, Fig. 3(a), a coherent attribution because the atmosphere used was inert (N_2). Subsequently, with the increase in temperature, intense peaks attributed to fragments of dimethoxybenzene and methoxybenzene are observed, Fig. 3(b, c), which continue to be released in decreasing proportion until the end of this step together with fragments of methanol and carbon dioxide. The slow mass loss steps, for both compounds, starting at 439 °C (La) and 416 °C (Ce), show peaks for the fragments only in the 3000 cm^{-1} region, corresponding to C—H group stretching that may indicate the presence of different sizes of carbon chain. Furthermore, it is more likely that these fragments originated from the aromatic skeleton, since it was not possible to observe bands related to benzene in the FT-IR spectra, considering the monitoring between 30 and 1000 °C performed for both compounds.

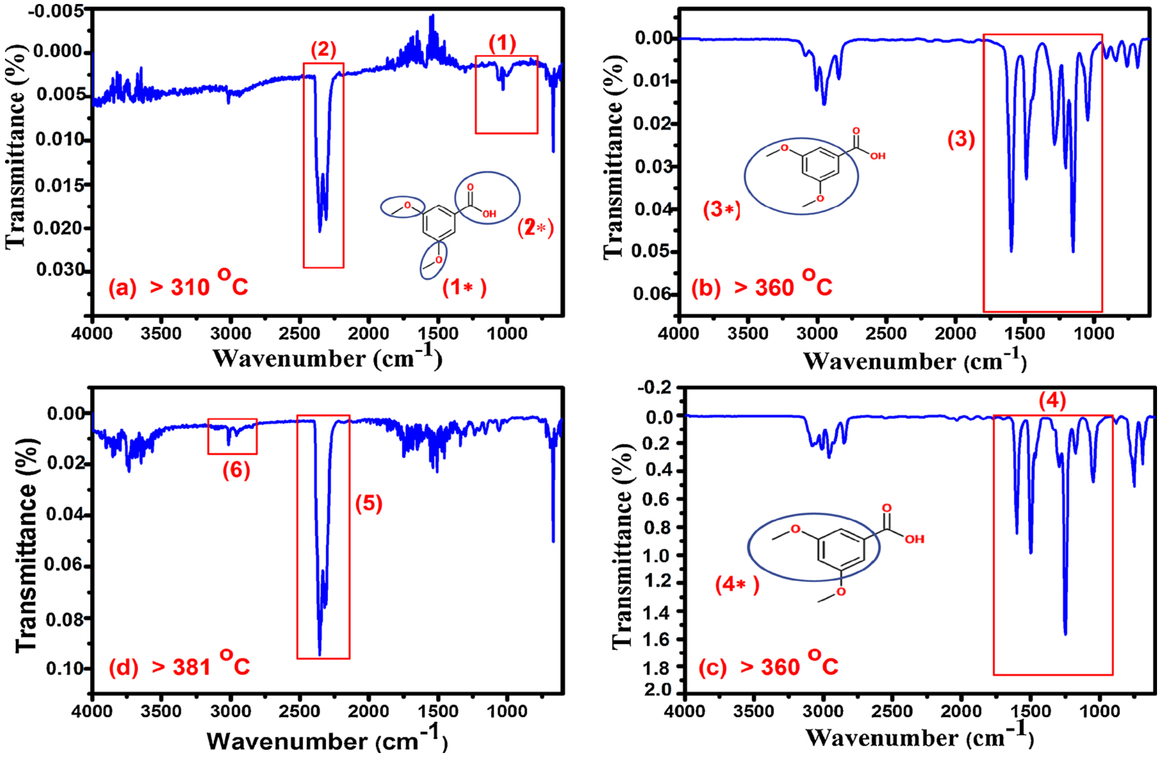

Fig. 3. a–d). FT-IR spectra of the main gaseous products monitored in air and N_2 atmospheres from the thermal decomposition of the complexes [La$(DMBz)_3$·$2H_2O$] and [Ce$(DMBz)_3$] at the temperatures (TGA): (a) > 310 °C (b and c) > 360 to 400 °C and (d) above 381 °C. DMBz: 3,5-dimethoxybenzoate.

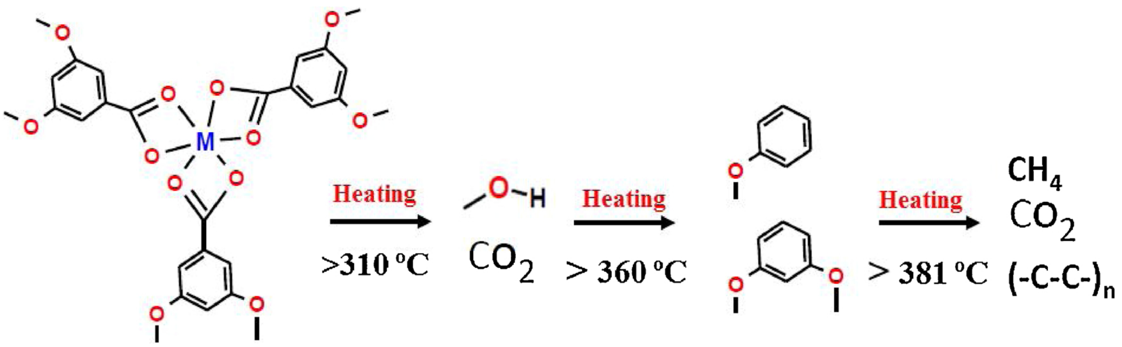

Fig. 4. Illustration based on the most products released, for the main path thermal decomposition follows in lanthanum and cerium 3,5-methoxybenzoate complexes, monitored by TGA-DSC / FT-IR in air and nitrogen atmospheres.

This statement can be made due to the absence of characteristic bands of benzene, located in 1802 and 1950 cm^{-1}. From these data, it was possible to qualitatively suggest, based on the gaseous products released in greater quantity, the main way in which fragmentation occurs, as shown in simplified form in Fig. 4.

3.2. Structural study

3.2.1. Infrared spectroscopy: theoretical and experimental

The experimental and theoretical FT-IR spectra for the ligand salt and lanthanum complex, as representatives of both complexes, are shown in Fig. 5 due to similarity of spectra. The optimized structures used to generate the theoretical vibrational spectra are shown in the supplementary material, Fig. S2. The identification of the main bands in the FT-IR spectra, Table 2, was performed from the spectroscopic correlations by computational animations and by checking the level of correspondence with the FT-IR experimental data. As it can be observed in Fig. 5, the positions of the main bands between the theoretical (a*, b*) and experimental (a, b) spectra are highly concordant, suggesting that the proposed structures are very close to the real structure. However, due to the approximate nature of the computational technique, small differences observed were expected, since the theoretical calculations do not include harmonic effects in the infrared vibrations, besides the complexes have been considered in the gaseous phase for the calculations [35]. In this work, as the experimental infrared spectra of the complexes are very similar, that allows us to state that the coordination occurs equally for both compounds.

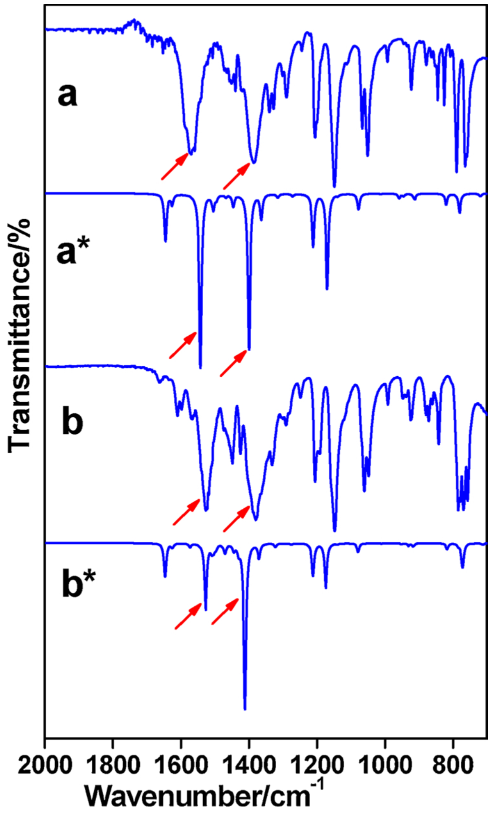

Fig. 5. Experimental FT-IR spectra of the 3,5-dimethoxybenzoate sodium salt (a) and lanthanum complex (b), correlated to the FT-IR theoretical spectra of 3,5–dimethoxybenzoate sodium salt (a*) and lanthanum complex (b*). The lanthanum complex was used as representative of cerium complex due to their similarity.

Table 2
Experimental and theoretical FT-IR data assigned to the 3,5-dimethoxybenzoate salt and lanthanum 3,5-dimethoxybenzoate complex as representative of all complexes.

Assignment	NaDMBz		$[La(DMBz)_3{\cdot}2H_2O]$	
	Exp.	Theor.	Exp.	Theor.
ν C = C (ring)	1653_w, 1340_m	1645, 1363	1610_m, 1331_m	1646, 1371
δ CH_3 + δ C– H (ring) + ν C–OCH_3	1205_s, 1148_s	1211, 1170	1202_m, 1148_s	1211, 1174
ν_{asym} COO–	1561_s	1542	1526_s	1527
ν_{sym} COO–	1385_s	1399	1381_s	1412
$\Delta\nu$ ($\nu_{asym} - \nu_{sym}$)	176	157	145	115

ν: stretching vibration; δ: bending vibration; asym: asymmetrical; sym: symmetrical; w: weak; m: medium; S: Strong; Theor.: Theoretical; Exp.: Experimental; DMBz: 3,5–dimethoxybenzoate.

In order to study the coordination mode of the carboxylate groups to the metal centers, as indicated by the experimental and theoretical calculation results, the methodology described by Deacon and Phillips [36] was applied. The differences between the symmetric and asymmetric stretching values for carboxylate groups of complexes and the ionic compound (sodium salt) were compared. From the combined results, presented in Table 2, it can be suggested that the carboxylate group is coordinated to the lanthanide ions by bidentate chelating mode [33–35]. In addition to the complexation study by FT-IR data, further X-ray powder diffraction is intended to provide accurate structural information on the crystalline structures.

3.3. Crystalline structure

In the absence of suitable single crystals, the complexes were previously characterized by thermogravimetry and simultaneous differential scanning calorimetry (TGA-DSC) to determine stoichiometric ratio and thermal stability. From this data, the structural arrangement was determined using X-ray powder diffraction after dehydration of lanthanum compound at 200 °C.

Table 3
Principal data of crystalline parameters obtained for [Ce(DMBz)$_3$] and [La(DMBz)$_3$] complexes.

	[Ce(DMBz)$_3$]	[La(DMBz)$_3$]
Empirical formula	$C_{27}H_{27}O_{12}Ce$	$C_{27}H_{27}O_{12}La$
Formula weight (gmol^{-1})	683.61	682.40
T(K)	298	298
λ(CuKα) (Å)	1.5418	1.5418
Crystal system	Monoclinic	Monoclinic
Space group	$P2_1/c$	$P2_1/c$
a(Å)	14.829(8)	14.790(1)
b,(Å)	24.351(2)	24.294(3)
c(Å)	7.7758(1)	7.836(2)
$\alpha=\gamma$ (^{o})	90	90
β (^{o})	97.85(6)	98.16(1)
V (Å^3)	2775.2(4)	2787.0(9)
Z	4	4
d$_{calc}$(g cm^{-3})	1.636(2)	1.626(5)
μ (mm^{-1})	13.2(8)	12.4(4)
Number of parameters	78	73
R_{Bragg}, R_{wp}	0.069 / 0.0106	0.0359 / 0.0827

Table 4
Main Ln-O bond lengths of oxygen atoms around lanthanide ions (Ln).

[Ce(DMBz)$_3$]			
Lengths/Å			
O11	2.420(2)	O31	2.597(2)
O12	2.618(3)	O32	2.459(3)
O21	2.466(2)	O32^i	2.718(1)
O22	2.629(3)		
[La(DMBz)$_3$]			
O11	2.501(5)	O31	2.541(2)
O12	2.585(3)	O32	2.394(3)
O21	2.232(3)	O11^i	2.733(2)
O22	2.648(3)		

The crystal structure models of the [La(DMBz)$_3$] and [Ce(DMBz)$_3$] complexes in anhydrous form were solved using state-of-the-art powder diffraction data measured in conventional laboratory equipment. In order to solve the present crystal structures, a rigid body for organic moiety and a high number of parameters were extensively used. After a long procedure as described before, very important crystallochemical information could be afforded and the crystallographic parameters of both complexes were summarized in Table 3, while the eight oxigen-lanthanides bond distances present in the coordination sphere of cerium and lanthanum are given in Table 4. The molecular structure of both complexes, drawn using OLEX2 [37], are shown in Fig. 6(a, b), as well as the overall packing and hydrogen bond are presented in Figures S3 (a–d) and S4 (a–e) as supplementary material. The DMBz is a carboxylate ligand and there are three coordination modes for carboxylate ligands [16,17]. The bidentate chelating (mode a) is easily described as both oxygen atoms bonded to the same lanthanide ion. Another coordination mode is when a lanthanide ion carboxylate forms a monoatomic bridge or μ-oxo bridge (mode b). The third mode is when each oxygen in a carboxylate group binds to a different lanthanide ion, syn, syn-η1:η1:μ2 bidentate bridging fashion.

As described in Fig. 6(a, b), both structures show two ligands bonded to lanthanide ions through the carboxylate group in mode a and b only the other DMBz ligand is coordinated to lanthanide ion in mode b. Besides the lanthanide-oxigen bond lengths, both complexes also exhibit important and strong interaction, that is, 3.879 Å and 3.944 Å, between Ce-Ce and La-La metal ions respectively.

In the supplementary material, Figures S3 and S4 show the main hydrogen bonds for the [Ce(DMBz)$_3$] and [La(DMBz)$_3$] complexes, respectively. For [La(DMBz)$_3$], there are intramolecular H-bonds between H11 and H21 with O21, H31 and H38b with O31 and O32 with H21 and two other intermolecular H-bonds between H33…O64 and H13…O63. Similarly, H-bonds fashion are observed in [Ce(DMBz)$_3$], where the two intermolecular H-bonds are assembled by O31…H31 and O54…H18a and the intramolecular ones are located between O12…H21 and O31…H31.

3.4. UV–vis absorption study

For both complexes studied, the electronic experimental spectra recorded in DMF solution show a single absorption band that reaches its maximum at 298 nm. For the DFT calculations, unfolding in two bands of different intensities in the UV–vis spectra is observed; an intense band at 255 nm and a lower intensity one at 300 nm, as shown in Fig. 7, so that such differences may probably be due to experimental conditions like complex-solvent interaction or even by limitation of the monochromator system (bandpass limitation) in the equipment used. In addition, for the theoretical calculations a single molecule, free of interactions, is taken into account.

From HOMO → LUMO orbital transitions, Fig. S5, it is noticed that

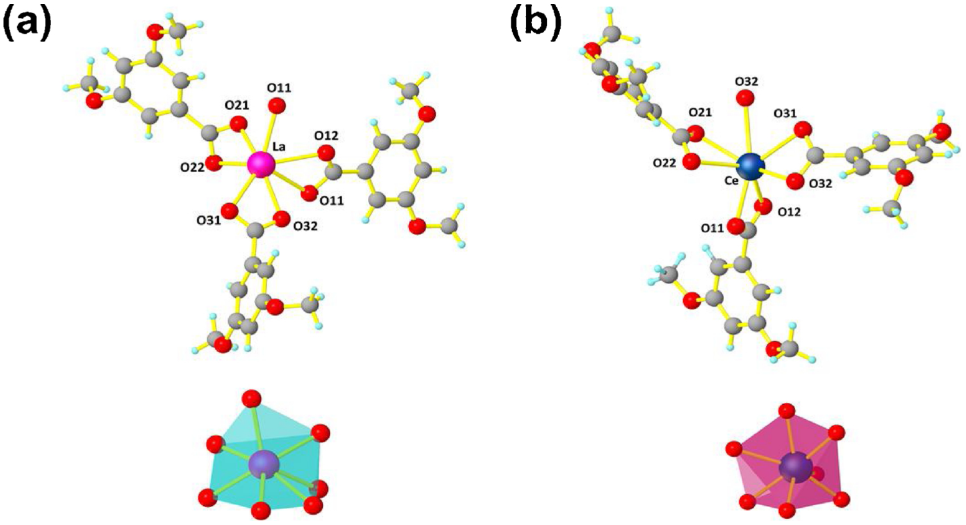

Fig. 6. (a, b). Asymmetric units and distorted pentagonal bipyramidal geometry around (a) La^{3+} and (b) Ce^{3+} respectively. Ln-O bonds are represented in both structures, whereas Ln represents La^{3+} and Ce^{3+} lanthanide ions.

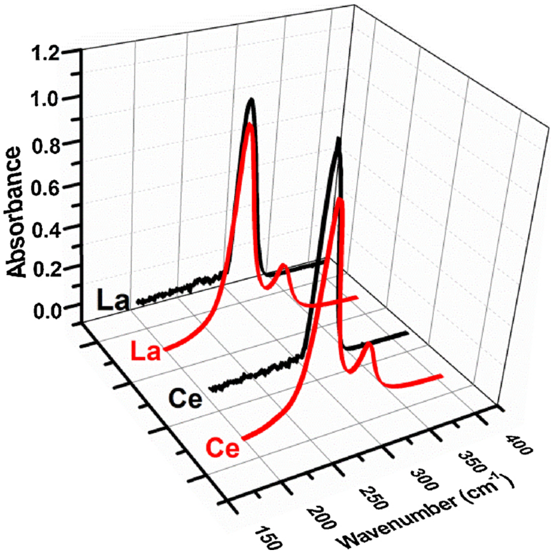

Fig. 7. Absorption spectra in UV–vis (experimental: black; theoretical: red) for the [La(DMBz)$_3$·2H$_2$O] and [Ce(DMBz)$_3$] complexes. DMBz: 3,5-dimethoxybenzoate (For interpretation of the references to colour in this figure legend, the reader is referred to the web version of this article).

the charge density on the organic part of the complex is due to π-π* and n-π* transitions, the latter being usually of low intensity. According to literature, π-π* transitions for organic ligands are recorded in the region between 196 and 313 nm and correspond to the C═C chromophore group of aromatic ring [38]. The overlapped band in the UV–vis experimental data, apparent at 300 nm in the theoretical calculation, is probably due to n-π* transitions. Regarding the charge transfer on the metal complexes, the overlapping of oxygens p-orbital of the carboxylate group (Fig. S5) should have favored the interligand charge transfer like in HOMO + 1 → LUMO (74 %), HOMO + 2 → LUMO (89 %) for lanthanum and HOMO + 1 → LUMO (69 %), HOMO + 2 → LUMO (89 %) for cerium. The main contributions of UV–vis radiation absorption occur through the aromatic system and the carboxylate group interactions, although singlet states of charge transfer of ligand-metal can also contribute. Anyway, those contributions are discussed in the fluorescence section.

3.5. Fluorescence study

The molecular orbitals (HOMO/LUMO) with the highest probability of charge transfer on the 3,5-dimethoxybenzoate lanthanum and cerium complexes were obtained by Time-Dependent Density Functional (TD-DFT) Theory. However, lanthanum (III) ion, in contrast to other lanthanide ions, is theoretically non-fluorescent because of its $3d^{10}4f^{\circ}$ electronic configuration, so only the fluorescence for the cerium complex is discussed in this section. The emission (fluorescence) of the Ce (III) results from 4f-5d optical transitions, which gives rise to much more intense bands than intraconfiguration transitions of 4f-4f type and the emission is generally observed in the ultraviolet region, although it may also occur in the visible region [39].

In Fig. 8(a, b), the major HOMO →LUMO orbitals contributions and experimental excitation and emission spectra are shown, which are correlated with each other to identify the electronic transitions responsible for the system's fluorescence. The H-1(93 %) and H-2(98 %) → L + 3 transitions (Fig. 8(a)) show that there is one ligand-metal charge transfer (LMCT), as well as contributions of intraligand charge transfer (ILCT and LMCT) originated from a mixture of transitions H-1(69 %); H-2 (88 %); H-4 (93 %) and H-5 (86 %) → LUMO. The contributions ILCT and LMCT, especially the LMCT, can be justified since the orbital of the organic part of the molecule has also charge distribution on the metallic center. In addition, from the experimental and theoretical data (Fig. 8(a,b)) and summary in Table S2), we have not excluded the possibility of ligand-ligand charge transfer (LLCT) as a function of this overlapping of orbitals on the metallic center.

The excitation and emission spectra, Fig. 8(b), were obtained respectively by monitoring of λ_{max} at 310 nm and λ_{max} emission at 355 nm. Hence, the emission band in the spectrum observed at 355 nm is an overlapping (summation) of n-π* and π-π* transitions of the ligand, as well as LMCT contributions from the antenna effect, transitions attributed to energy levels of the Ce(III) metal center $^2F_{7/2} \rightarrow {}^2F_{5/2}$.

4. Conclusions

The lanthanum(III) and cerium(III) complexes using a monocarboxylate ligand, 3,5-methoxybenzoate, were synthesized in aqueous medium and characterized in the solid state or solution by thermoanalytical methods, X-ray diffraction, FT-IR and UV–vis.

Based on the thermoanalytical data from the TGA-DSC curves, it was possible to define the stoichiometric ratio of the synthesized complexes as M(DMBz)$_3$, where M represents the lanthanides and DMBz the 3,5-dimethoxybenzoate ligand. Among the complexes synthesized and characterized, only that of lanthanum was obtained in hydrated form. A probable explanation can be attributed to the lower lanthanide contraction effect for lanthanum, which would make the coordination sphere more available. Another relevant information from TGA-DSC/DTG to the study of these materials was the thermal stability, decomposition temperatures, as well as the temperature of formation of the

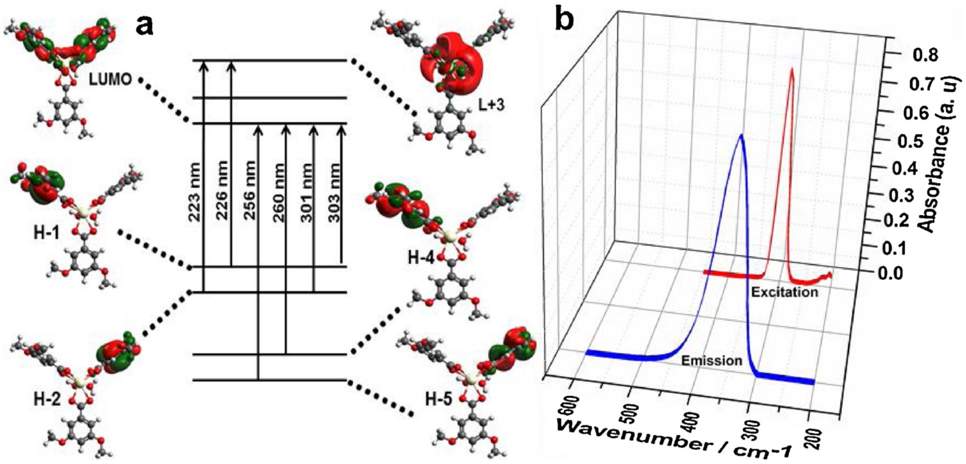

Fig. 8. (a) Molecular orbitals for [Ce(DMBz)$_3$] according to the TD-DFT calculations, (b) excitation and emission spectra in. UV–vis.

final residue used in the calculation of stoichiometry and the monitoring, by TGA/FT-IR, of the main volatile products related to thermal decomposition and consequently the probable path thermal decomposition follows.

From FT-IR spectroscopic data, it can be suggested that the 3,5-dimethoxybenzoate monocarboxylate ligand coordinates with lanthanide ions in chelating form, while by X-ray diffractograms with Rietveld refinement, it was possible to establish that the monocarboxylate ligand coordinates both in chelating and bridge forms. The result of this coordination mixture generated polymeric and practically isomorphic structures for the complexes, defined as $[M(DMBz)_3]n$ with a monoclinic system of space group $P2_{1/c}$. For cerium(III) complex, through UV–vis absorption calculations using the TD-DFT theory, it was possible to suggest that the charge transfer orientations, according to HOMO and LUMO orbitals, occur by antenna effect of the ligand for $^2F_{7/2}$ and $^2F_{5/2}$ energy levels of the metal ion.

In summary, it is concluded that monocarboxylate ligands can also generate polymeric structures with lanthanide ions as shown in this study. In this sense, it is possible that certain properties, such as those of fluorescence, are altered depending on the type of coordination and/or crystalline structure, as well as on the experimental conditions of synthesis employed. However, this study limited itself to the synthesis, elucidation of the stoichiometry and crystalline structure of the complexes obtained in crystalline powder form.

Declaration of interests

The authors declare that they have no known competing financial interests or personal relationships that could have appeared to influence the work reported in this paper.

Acknowledgements

The authors thank the Brazilian Foundations CNPQ (grant nº 434138/2018-5), FUNDECT, CAPES and FINEP (Contract: 04.13.0448.00/2013) for financial support, and are grateful to Professor Massao Ionashiro for allowing us to carry out measurements in the Ivo Giolito Thermal Analysis Laboratory (LATIG) – UNESP. Daniel M. Brasil and Leandro M. C. Pinto acknowledge CENAPAD–SP (Centro Nacional de Processamento de Alto Desempenho em São Paulo) for granting computing time and Professional Noemi Marques de Carvalho for English reviewing.

Appendix A. Supplementary data

Supplementary material related to this article can be found, in the online version, at doi:https://doi.org/10.1016/j.tca.2020.178662.

References

[1] C.T. Carvalho, G.F. Oliveira, J. Fernandes, A.B. Siqueira, E.Y. Ionashiro, M. Ionashiro, Rare-earth metal compounds with a novel ligand 2-methoxycinnamylidenepyruvate: a thermal and spectroscopic approach, Thermochim. Acta 637 (2016) 17–23, https://doi.org/10.1016/j.tca.2016.05.008.

[2] A.L.C.S. do Nascimento, J.A. Teixeira, W.D.G. Nunes, F.X. Campos, O. Treu-Filho, F.J. Caires, M. Ionashiro, Thermal behavior, spectroscopic study and evolved gas analysis (EGA) during pyrolysis of picolinic acid, sodium picolinate and its light trivalent lanthanide complexes in solid, J. Anal. Appl. Pyrolysis 119 (2016) 242–250, https://doi.org/10.1016/j.jaap.2016.01.010.

[3] W. Ferenc, A. Walków-Dziewulska, J. Chruciel, Spectral and thermal behaviours of rare earth element complexes with 3,5-dimethoxybenzoic acid, J. Serb. Chem. Soc. 68 (2003) 751–763.

[4] J. sienkiewicz-gromiuk, I. Rusinek, L. Kurach, Z. Rzaczynka, Thermal and spectroscopic \(I.R., XPS) properties of lanthanide(III) benzene-1,3,5-triacetate complexes, J. Therm. Anal. Calorim. 126 (2016) 327–342, https://doi.org/10.1007/s10973-016-5521-8.

[5] R. Decadt, K.V. Hecke, D. Depla, K. Leus, D. Weinberger, I.V. Driessche, P.V. Der Voort, R.V. Deun, Synthesis, crystal structures, and luminescence properties of carboxylate based rare-earth coordination polymers, Inorg. Chem. 51 (2012) 11623–11634, https://doi.org/10.1021/ic301544q.

[6] Z. Ling-Yan, R. Li, L. Li-Wei, W. Li-Na, Synthesis, structure, and character of two rare earth carboxylic acid complexes, J. Coord. Chem. 70 (2017) 4008–4018, https://doi.org/10.1080/00958972.2017.1415431.

[7] J.-Ru Zheng, N. Ren, Jian-Jun Zhang, Da-Hai Zhang, Li-Zhen Yan, Shu-Ping Wang, Crystal structures, luminescence, and thermodynamic properties of lanthanide complexes with 3,5-dimethoxybenzoic acid and 1,10-phenanthroline, J. Chem. Thermodyn. 57 (2013) 169–177, https://doi.org/10.1016/j.jct.2012.08.015.

[8] Yan-Zu Du, Jin-Min Zheng, Syntheses, structures and magnetic properties of a series of lanthanide complexes based on p-methoxybenzoic acid, Inorg. Chem. Commun. 66 (2016) 59–63, https://doi.org/10.1016/j.inoche.2016.01.020.

[9] Xiao-Xia Qi, Wu Jun-Chen, NingRen, Chun-Li Zhao, Jian-Jun Zhang, Guang-Cai Zong, Jie Gao, Novel lanthanide complexes constructed from 3,4-dimethoxybenzoic acid: crystal structures, spectrum and thermochemical properties, Thermochim. Acta 615 (2015) 1–7, https://doi.org/10.1016/j.tca.2015.07.003.

[10] K.V. Tenório, J.A. Teixeira, L.M.C. Pinto, F.J. Caires, O. Treu-Filho, F.A. Santos, T.A.D. Colman, A. Cuin, C.T. Carvalho, Synthesis and structure of a praseodymium (III) complex with carboxylate ligand: a thermal and spectroscopic study, J. Rare Earths (2018) 1–8, https://doi.org/10.1016/j.jre.2018.03.019.

[11] A.A. Coelho, Indexing of powder diffraction patterns by iterative use of singular value decomposition, J. Appl. Cryst. 36 (2003) 86–95, https://doi.org/10.1107/S0021889802019878.

[12] (TOPAS-R). Version 4.2, General Profile and Structure Analysis Software for Powder Diffraction Data (Bruker AXS, Karlsruhe, Germany), 2009.

[13] G.S. Pawley, Unit–cell refinement from powder diffraction scans, J. Appl. Cryst. 14 (1981) 357–361, https://doi.org/10.1107/S0021889881009618.

[14] A.L. Spek, Structure validation in chemical crystallography, Acta Cryst. 65 (2009) 148–155, https://doi.org/10.1107/S090744490804362X.

[15] A.A. Coelho, Whole-profile structure solution from powder diffraction data using simulated annealing, J. Appl. Cryst. 22 (2000) 899–908, https://doi.org/10.1107/S002188980000248X.

[16] D.E. Lynch, G. Smith, K.A. Byriel, C.H.L. Kennard, 3,5–dimethoxybenzoic acid and the second polymorph of the 2:1 adduct of 3,5-dinitrobenzoic acid with ethylenediamine, Acta Cryst. 50 (1994) 1259–1262, https://doi.org/10.1107/S0108270193012259.

[17] L.F. Marques, A. Cuin, G.S.G. de Carvalho, M.V. dos Santos, S.J.L. Ribeiro, F.C. Machado, Energy transferprocess in highly photoluminescent binuclear hydrocinnamate of europium, terbium 1,10-phenanthroline as ancillary ligand, Inorg. Chim. Acta Rev. 441 (2016) 67–77, https://doi.org/10.1016/j.ica.2015.11.009.

[18] T.C. de Oliveira, H.P. Santos, M.G. Lahoud, D.F. Franco, R.O. Freire, J.D.L. Dutra, A. Cuin, J.F. de Lima, L.F. Marques, Elucidating the energy transfer process in mononuclear and binuclear lanthanide complexes of the anti-inflammatory drug ibuprofen: From synthesis to high luminescence emission, J. Lumin. 181 (2017) 196–210, https://doi.org/10.1016/j.jlumin.2016.09.024.

[19] R.A. Young, The Rietveld Method. (IUCr Monograph No 5), Oxford University Press, New York, 1981.

[20] A.D. Becke, Thermochemistry. III. The role of exact exchange, J. Chem. Phys. 98 (1993) 5648–5652, https://doi.org/10.1063/1.464913.

[21] C. Lee, W. Yang, R.G. Parr, Development of the Colle-Salvetti correlation-energy formula into a functional of the electron density, Phys. Rev. B 37 (1988) 785, https://doi.org/10.1103/PhysRevB.37.785-789.

[22] M.J. Frisch, G.W. Trucks, H.B. Schlegel, G.E. Scuseria, M.A. Robb, J.R. Cheeseman, G. Scalmani, V. Barone, et al., Gaussian 09, Revision A.02, Gaussian, Inc., Wallingford CT, 2009.

[23] D.Z. Goodson, S.K. Sarpal, P. Bopp, M. Wolfsberg, Influence on isotope effect calculations of the method of obtaining force constants from vibrational data, J. Phys. Chem. 86 (1982) 659–663, https://doi.org/10.1021/j100394a014.

[24] J. Bertrán, I.G. Csizmadia, New Theoretical Concepts for Understanding Organic Reactions, first ed., Springer, Netherlands, 1989, https://doi.org/10.1007/978-94-009-2313-3.

[25] R. Dennington, T. Keith, J. Millam, Gauss View. Shawnee Mission, Semichem. Inc., Version 5.0.8, KS, 2009.

[26] F. Weigend, R. Ahlrichs, Balanced basis sets of split valence, triple zeta valence and quadruple zeta valence quality for H to Rn: design and assessment of accuracy, Phys. Chem. Chem. Phys. 7 (2005) 3297–3305, https://doi.org/10.1039/B508541A.

[27] M. Dolg, H. Stoll, A. Savin, H. Preuss, Energy-adjusted pseudopotentials for the rare earth elements, Theor. Chim. Acta 75 (1989) 173–194, https://doi.org/10.1007/BF00528565.

[28] M. Dolg, H. Stoll, H. Preuss, A combination of quasirelativisticpseudopotential and ligand field calculations for lanthanoid compounds, Theor. Chim. Acta 85 (1993) 441–450.

[29] F. Neese, The ORCA program system, Wiley Interdisc. Rev. – Comput. Mol. Sci. 2 (2012) 73–78, https://doi.org/10.1002/wcms.81.

[30] M.D. Hanwell, D.E. Curtis, D.C. Lonie, T. Vandermeersch, E. Zurek, G.R. Hutchison, Avogadro: an advanced semantic chemical editor, visualization, and analysis platform, J. Cheminformatics. (2012) 1–17, https://doi.org/10.1186/1758-2946-4-17.

[31] C.F. Almeida, R.C. Andrade, L.W. Aguiar, F.J. Caires, E.A. Falcão, C.T. Carvalho, Thermal and spectroscopic study of the lanthanide 2-aminoterephthalate compounds in the solid state, J. Therm. Anal. Calorim. 117 (2014) 251–258, https://doi.org/10.1007/s10973-014-3721-7.

[32] P. Janoš, T. Hladík, M. Kormunda, J. Ederer, M. Šťastný, Thermal Treatment of Cerium Oxide and Its Properties: Adsorption Ability Versus Degradation Efficiency, (2014), https://doi.org/10.1155/2014/706041.

[33] R.M. Silverstein, F.X. Webster, D.J. Kiemle, Spectrometric Identification of Organic Compounds, 7th ed., John Wiley & Sons, Hoboken, 2005.

[34] K. Nakamoto, Infrared and Raman Spectra of Inorganic and Coordination

Compounds, 4th ed., Wiley, New York, 1986.

[35] J.G. Smith, Chapter 13 mass spectrometry and infrared spectroscopy, Organic Chemistry, 3rd ed., McGraw-Hill, New York, NY, 2011.

[36] G.B. Deacon, R.J. Phillips, Relationships between the carbon-oxigen stretching frequencies of carboxylate complexes and the type of carboxylate coordination, Coord. Chem. Rev. 33 (1980) 227–250, https://doi.org/10.1016/S0010-8545(00)80455-5.

[37] O.V. Dolomanov, L.J. Bourhis, R.J. Gildea, J.A.K. Howard, H. Puschmann, OLEX2: a complete structure solution, refinement and analysis program, J. App. Cryst. 42 (2009) 339–341, https://doi.org/10.1107/S0021889808042726.

[38] Heinz-Helmut Perkampus, UV-VIS Spectroscopy and Its Applications, Ed., Springer Science & Business Media, 2013.

[39] S.V. Eliseeva, J.C.G. Buunzli, Rare earths: jewels for functional materials of the future, New J. Chem. 35 (2011) 1165–1176, https://doi.org/10.1039/c0nj00969e.